Volume 7 | Number 13 | 7 July 2023

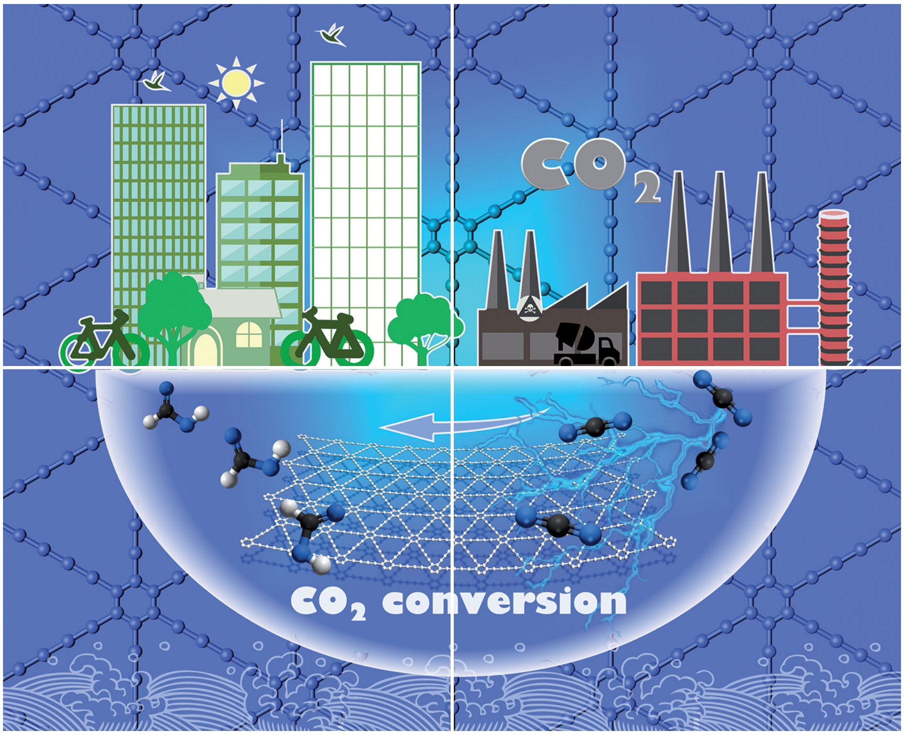

MATERIALS CHEMISTRY FRONTIERS

CCS 中国化学会 CHINESE CHEMICAL SOCIETY
ICCAS
ROYAL SOCIETY OF CHEMISTRY
rsc.li/frontiers-materials

MATERIALS CHEMISTRY FRONTIERS

RESEARCH ARTICLE

View Article Online
View Journal | View Issue

Check for updates

Cite this: *Mater. Chem. Front.*, 2023, 7, 2620

Graphdiyne/copper sulfide heterostructure for active conversion of CO_2 to formic acid†

Shiyao Cao,[a] Yurui Xue,*[ab] Xi Chen,[ac] Chao Zhang,[ac] Yang Gao[ac] and Yuliang Li*[ac]

Received 9th March 2023, Accepted 28th March 2023

DOI: 10.1039/d3qm00245d

rsc.li/frontiers-materials

The synthesis of electrocatalysts with high selectivity, activity, and stability for the CO_2 reduction reaction (CO_2RR) is a promising and sustainable route to convert CO_2 into value-added chemicals at room temperatures and pressures. Here we report a new heterostructured electrocatalyst of graphdiyne/copper sulfide (GDY/CuS_x) *via* the controlled *in situ* growth of GDY on the surface of CuS_x. Our results show that the introduction of GDY can effectively induce the formation of mixed-valence Cu(I, II) and incomplete charge transfer between the GDY and Cu atoms, which enhance the conductivity, produce new active sites, and finally result in a higher catalytic performance. In addition, the GDY grown on the surface of the catalysts endows the sample with a high long-term stability. Benefitting from above advantages, GDY/CuS_x shows a high CO_2-to-formate conversion performance with a high faradaic efficiency (FE) and long-term stability at room temperatures and ambient pressures.

1. Introduction

The electrocatalytic carbon dioxide reduction reaction (CO_2RR) at room temperatures and ambient pressures provides an effective route for the production of high-value-added chemicals and fuels from CO_2.[1–4] Formic acid (HCOOH), an important hydrogen carrier, plays an important role in the storage and transportation of hydrogen energy.[5–7] However, the catalysts reported for the CO_2RR suffer from sluggish kinetics due to the high overpotentials required to drive the CO_2RR process, in which the competing hydrogen evolution reaction (HER) occurs. Besides, the multi-proton/multi-electron transfer in the CO_2RR process commonly results in multiple types of gas- and/or liquid-phase products (carbon monoxide, methane, ethylene, formic acid, formaldehyde, methanol, ethanol, *etc.*).[8–10] These drawbacks of traditional catalysts lead to both low reaction selectivity and activity. During the past decades, many methods, such as alloying,[11] chemical doping,[12,13] catalyst surface modification,[14] *etc.*, have been reported to improve the performance of the electrocatalytic CO_2RR. The design and synthesis of new electrocatalysts that demonstrate high selectivity (faradaic efficiency (FE)), a high reaction rate (large current densities) and long-term stability for CO_2-to-HCOOH conversion are still of great significance.

Graphdiyne (GDY) is a new two-dimensional all-carbon network in which each benzene ring (sp^2-hybridized C) is connected *via* alkyne bonds (sp-hybridized C).[15] The specific sp-/sp^2-cohybridized structure of GDY endows it with many unique and fascinating properties that are superior to traditional carbon materials, *e.g.*, the presence of abundant carbon chemical bonds, large conjugated π structures, natural cavities, a favourable band gap, *etc.* More attractively, the highly uneven distribution of surface charges and incomplete charge transfer between GDY and metal atoms can produce more active sites and a higher intrinsic activity, and efficiently regulate the adsorption/desorption behaviour of reaction intermediates on active site surfaces. Another unique property of GDY is that its controlled growth on arbitrary substrates can be carried out under ambient conditions, which shows great advantages in the controlled synthesis of high-performance interface structures for catalysis.[15–21] GDY has brought new opportunities for transformative breakthroughs in many fields, including catalysis, energy, photoelectric conversion devices, intelligent information systems, life sciences, and so on.[22–45] These advantages make GDY an ideal material for the synthesis of highly active and selective catalysts for the CO_2RR.

In this work, we report the controlled synthesis of GDY/CuS_x heterostructured catalysts by using the advantage of GDY in that it can be grown on arbitrary substrate surfaces. Experimental results show that the incomplete charge transfer between GDY and copper atoms and the GDY-induced formation of mixed-

[a] *CAS Key Laboratory of Organic Solids, Beijing National Laboratory for Molecular Sciences, Institute of Chemistry, Chinese Academy of Sciences, Beijing 100190, P. R. China. E-mail: ylli@iccas.ac.cn*

[b] *Shandong Provincial Key Laboratory for Science of Material Creation and Energy Conversion, Science Center for Material Creation and Energy Conversion, School of Chemistry and Chemical Engineering, Institute of Frontier and Interdisciplinary Science Shandong University, Jinan 250100, P. R. China. E-mail: yrxue@sdu.edu.cn*

[c] *University of Chinese Academy of Sciences, Beijing 100049, P. R. China*

† Electronic supplementary information (ESI) available. See DOI: **https://doi.org/10.1039/d3qm00245d**

valence Cu species can produce more active sites and improve the catalytic selectivity and activity for the CO_2RR at room temperatures and ambient pressures.

2. Experimental section

2.1 Materials

Tetrahydrofuran, ethyl acetate, acetone, sodium chloride, *N*,*N*,*N′*,*N′*-tetramethylethylenediamine, pyridine, and thiourea were purchased from Beijing Reagent Company. The copper foam was cleaned using acetone, 3 M HCl, deionized water, and ethanol before use. All organic reagents are analytical reagents.

2.2 Catalyst synthesis

Synthesis of CuS_x. Freshly cleaned copper foam was placed in a stainless-steel autoclave containing 10 mL thiourea solution (1.445 mmol L^{-1}) and heated at 150 °C for 5 hours. After completion of the reaction, the sample was washed three times with ethanol and dried under vacuum.

Synthesis of GDY/CuS_x. The obtained CuS_x was placed in a reactor containing 6 mg mL^{-1} hexaethynylbenzene (HEB), 10 mL ethyl acetate, 10 mL dichloromethane and 1 mL pyridine for seven days. After completion of the reaction, the sample was washed thoroughly with dichloromethane and acetone and dried under vacuum.

Results and discussion

Fig. 1a shows the synthesis route for GDY/CuS_x. Using copper foam as the substrate, a three-dimensional porous CuS_x electrode was obtained through a simple hydrothermal reaction. The obtained CuS_x electrode was then used directly as the substrate

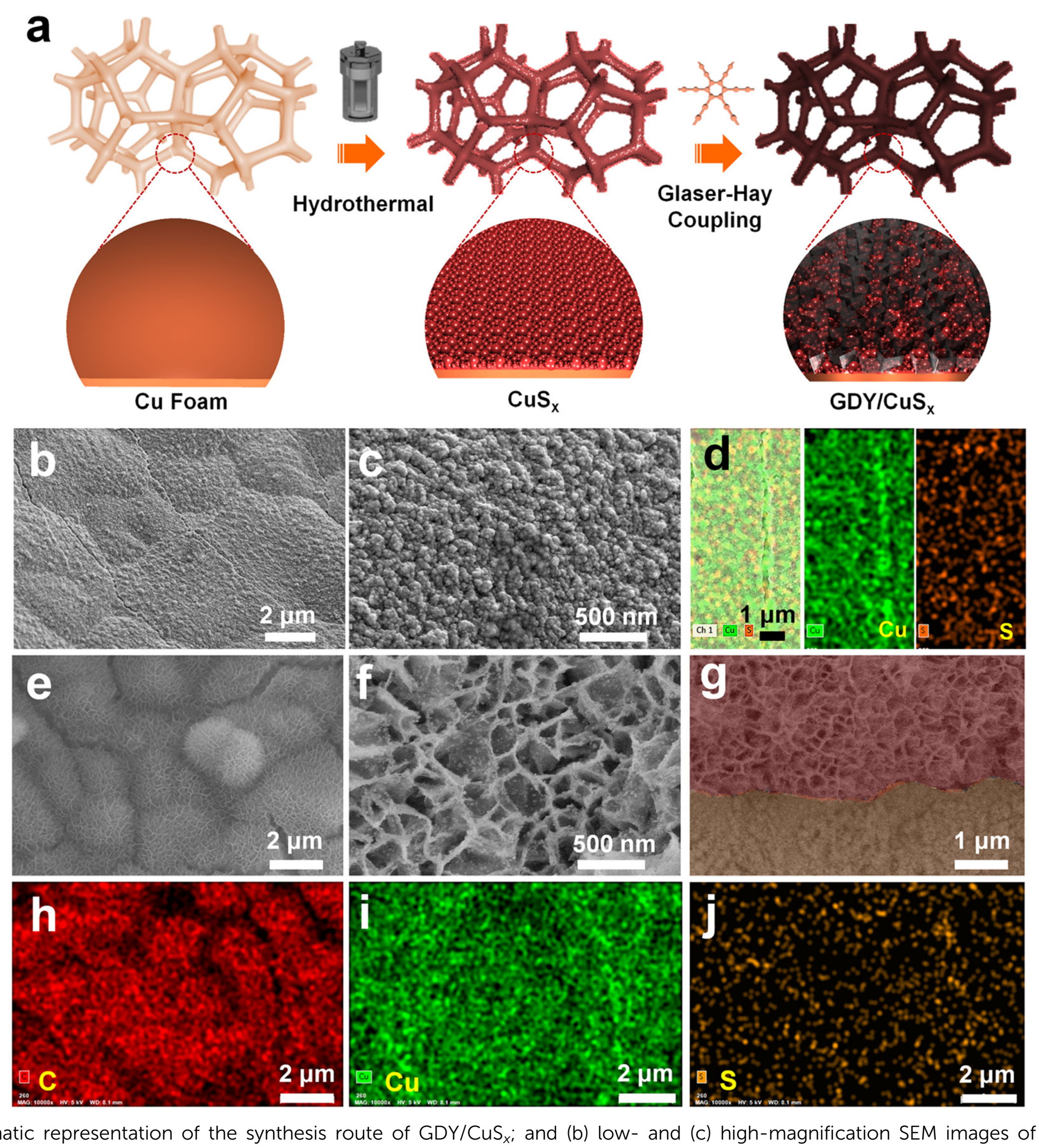

Fig. 1 (a) Schematic representation of the synthesis route of GDY/CuS_x; and (b) low- and (c) high-magnification SEM images of CuS_x. (d) Energy dispersive spectroscopy mapping of CuS_x. (e) Low- and (f) high-magnification SEM images of GDY/CuS_x. (g) Cross-section SEM image of GDY/CuS_x; and (h, i and j) energy dispersive spectroscopy mapping of GDY/CuS_x.

for the *in situ* growth of GDY *via* a cross-coupling reaction to synthesize the GDY/CuS_x heterostructure. Scanning electron microscopy (SEM) images (Fig. 1b and c) show that the surface of the copper foam (Fig. S1, ESI†) changed from smooth to porous with a granular distribution on the surface of the copper foam. Energy dispersive spectroscopy mapping of CuS_x (Fig. 1d) shows that the surface element components are Cu element and S element, which preliminarily confirms the successful synthesis of CuS_x. CuS_x acts as a catalyst for the cross-coupling reaction and a growth substrate for the controlled growth of GDY. After the Glaser–Hay coupling reaction, a film of GDY nanosheets with a three-dimensional porous morphology was formed on the surface of the CuS_x electrode (Fig. 1e and f). The cross-section image (Fig. 1g) further confirmed the successful growth of the GDY film on the surface of copper sulfide. X-ray energy dispersive spectra for GDY/CuS_x (Fig. 1h–j) reveal the presence and uniform distribution of C, Cu, and S elements in the catalyst.

The morphology of the samples was next characterized using transmission electron microscopy (TEM). As shown in Fig. 2a and b, the pure GDY electrode has a three-dimensional porous structure comprised of two-dimensional GDY nanosheets. The high-resolution TEM image (Fig. 2c) shows that the spacing distance of GDY is 0.335 nm. The elemental mapping images (Fig. 2d) show the uniform distribution of elemental C over the GDY nanosheets. For GDY/CuS_x, the three-dimensional porous morphology was well maintained (Fig. 2e) with nanoparticles uniformly distributed on the surface of GDY (Fig. 2f–h). The HRTEM image (Fig. 2i) shows that the growth of GDY on the CuS_x surface had occurred. The elemental mapping results of the GDY/CuS_x heterostructure (Fig. 2j–m) reveal the uniform distribution of the Cu, S, and C elements in the heterojunction catalyst. Moreover, full XPS survey spectra confirms the presence of C, Cu, S, and O elements in the sample (ESI,† Fig. S2) once again demonstrating the successful construction of the heterojunction catalyst.

XPS measurements were performed to determine the chemical structures of the samples. As shown in Fig. 3a, four peaks at 932.7/933.6 eV and 952.8/953.7 eV, which correspond to the +1 and +2 valences in Cu $2p_{3/2}$ and Cu $2p_{1/2}$, respectively, were observed from the high-resolution Cu 2p XPS spectra, revealing the mixed valence of copper in the GDY/CuS_x catalyst. Besides, the Cu 2p spectra of GDY/CuS_x showed a positive shift of 0.4 eV in binding energy compared with pure copper sulfide, which indicates the loss of electrons from Cu. For the C 1s XPS spectra (Fig. 3b), four characteristic peaks at 284.5 eV, 285.0 eV, 286.9 eV, and 288.5 eV, corresponding to C–C (sp^2-C), C–C (sp-C), C–O, and C═O, respectively, were observed. The area

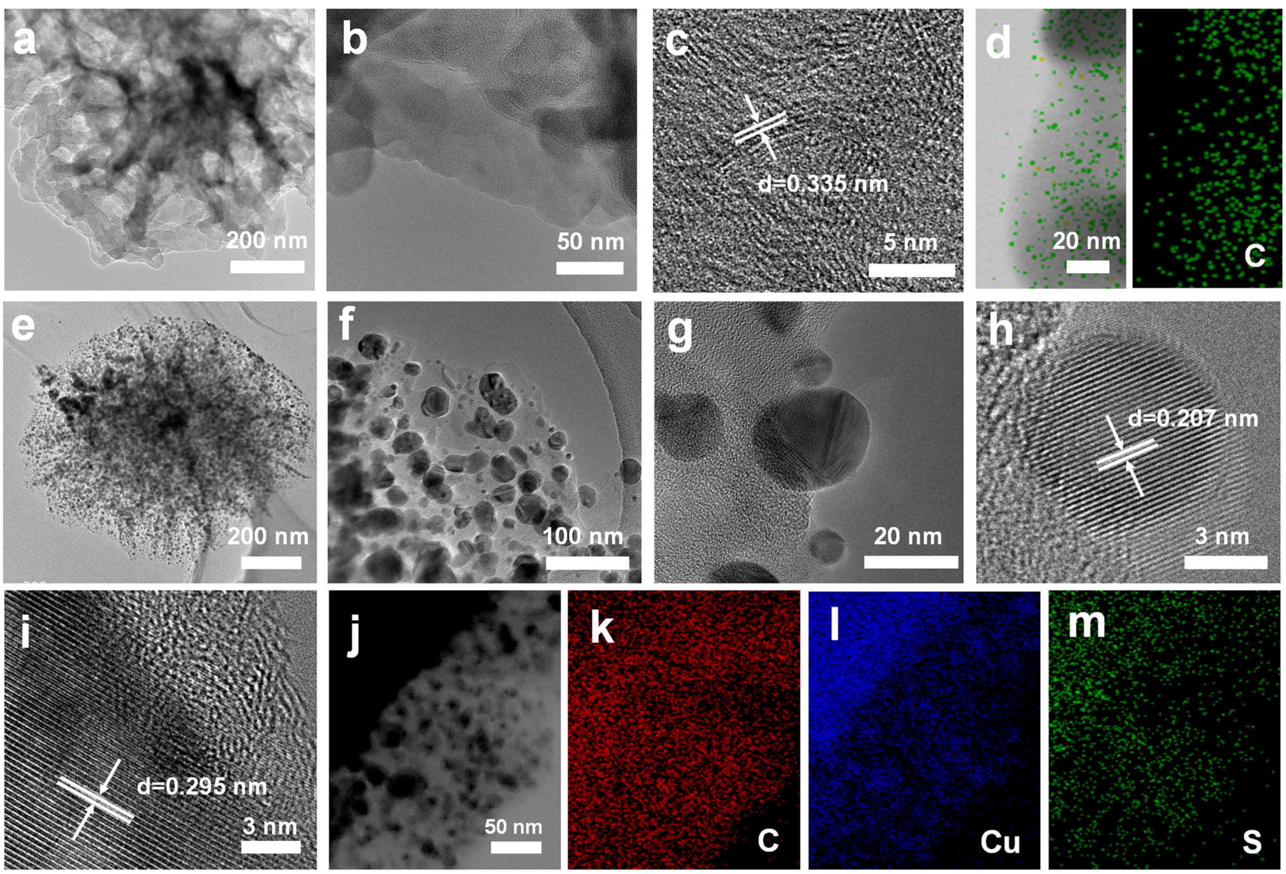

Fig. 2 (a) TEM and (b and c) HRTEM images of the GDY nanosheet. (d) STEM image (left) and corresponding elemental mapping (right) of the elemental C of GDY. (e–g) TEM and (h and i) HRTEM images of GDY/CuS_x, (j) STEM image and corresponding elemental mapping of (k) C, (l) Cu, and (m) S elements of the GDY/CuS_x electrode.

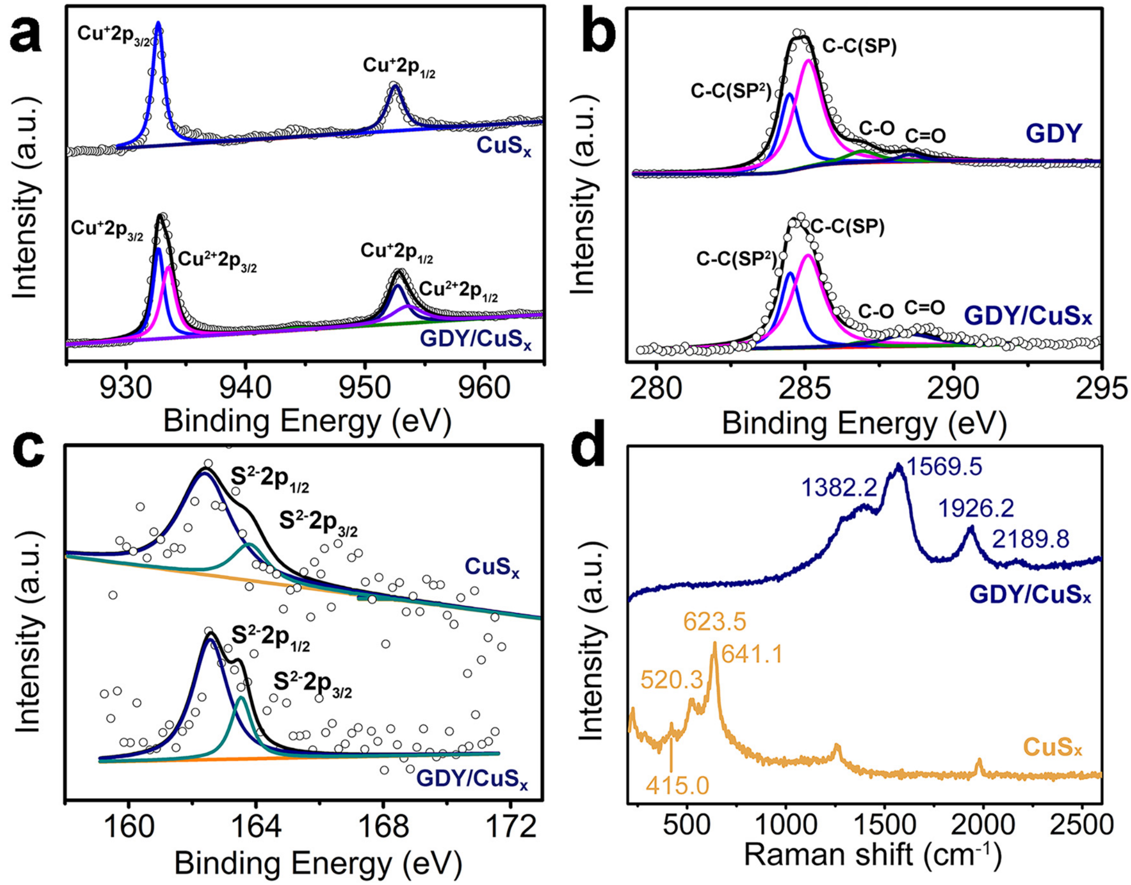

Fig. 3 High-resolution (a) Cu 2p, (b) C 1s, and (c) S 2p XPS spectra of CuS_x and GDY/CuS_x. (d) Raman spectra of CuS_x and GDY/CuS_x.

ratio of sp^2-C to sp-C peaks (0.5) for GDY/CuS_x is consistent with that of pure GDY. Compared with pure GDY, the peak of sp-C in GDY/CuS_x showed a negative shift of 0.2 eV, indicating that sp-C receives electrons. Fig. 3c shows the S 2p XPS spectra of the samples. The peak positions at 162.3 and 163.6 eV in the figure correspond to the two peaks of $S^{2-}2p_{3/2}$ and $S^{2-}2p_{1/2}$, respectively. The XPS results demonstrate the incomplete charge transfer between GDY and metal copper atoms, which is beneficial for enhancing the catalytic activity. The Raman spectra (Fig. 3d) show both the characteristic peaks of CuS_x and the characteristic peaks of graphdiyne, which further proves that the GDY/CuS_x heterojunction catalyst was successfully synthesized.

A three-electrode system was applied to test the electrocatalytic CO_2RR performance to formic acid in 0.1 M $KHCO_3$ electrolyte. Fig. 4a shows the linear sweep voltammetry (LSV) curves of the as-prepared samples. The current density of the GDY/CuS_x electrode in the CO_2-saturated 0.1 M $KHCO_3$ electrolyte is significantly larger than that in the Ar-saturated 0.1 M $KHCO_3$ electrolyte, which indicates that the GDY/CuS_x electrode has a clear carbon dioxide reduction ability. At the same potentials, the current density for GDY/CuS_x was larger than that of CuS_x. These results confirm that the introduction of GDY can significantly improve the CO_2RR activity of the catalyst. The electrolyte after the electrocatalytic CO_2RR at different voltages was analysed using NMR (Fig. 4b and c). The faradaic efficiency values of the gas phase products and liquid phase products of GDY/CuS_x under different bias voltages are shown in Fig. 4d. It was observed that the gas phase products were mainly hydrogen. Fig. 4e shows the potential-dependent FE and total current density of the CO_2RR to formic acid. GDY/CuS_x exhibits a high FE for formic acid production of 70% at −0.9 V *vs.* RHE, with a total current density reaching −65.6 mA cm^{-2}, which are better than that of pure CuS_x samples at the same potential (Fig. S3, ESI†). Overall, the side reaction of CO and hydrocarbon production has been significantly inhibited under the bias voltage of −0.9 V *vs.* RHE. Such a catalytic performance could be maintained over a 4 hour period (Fig. 4f). SEM images for the samples obtained after the stability test show that there is almost no variation in the morphology (Fig. S4, ESI†). *In situ* ATR-FTIR characterization was employed to identify the chemical structure of the intermediates involved during the electrochemical CO_2RR. As shown in Fig. 4g, after subtracting the background of the open circuit potential infrared spectrum, the intensity of three bands of 1640, 2100, and 2340 cm^{-1} can be observed. The strong positive band in the 1640 cm^{-1} region can be assigned to interfacial H_2O, which accumulates in the electrocatalyst due to catalysis or the increasing negative polarization of the electrode.[46] The positive strong band in the 2340 cm^{-1} region is attributed mainly to the adsorption of CO_2 on the electrode surface.[47] The positive band located in the 2100 cm^{-1} region observed between −0.7 V and −1.5 V *vs.* RHE

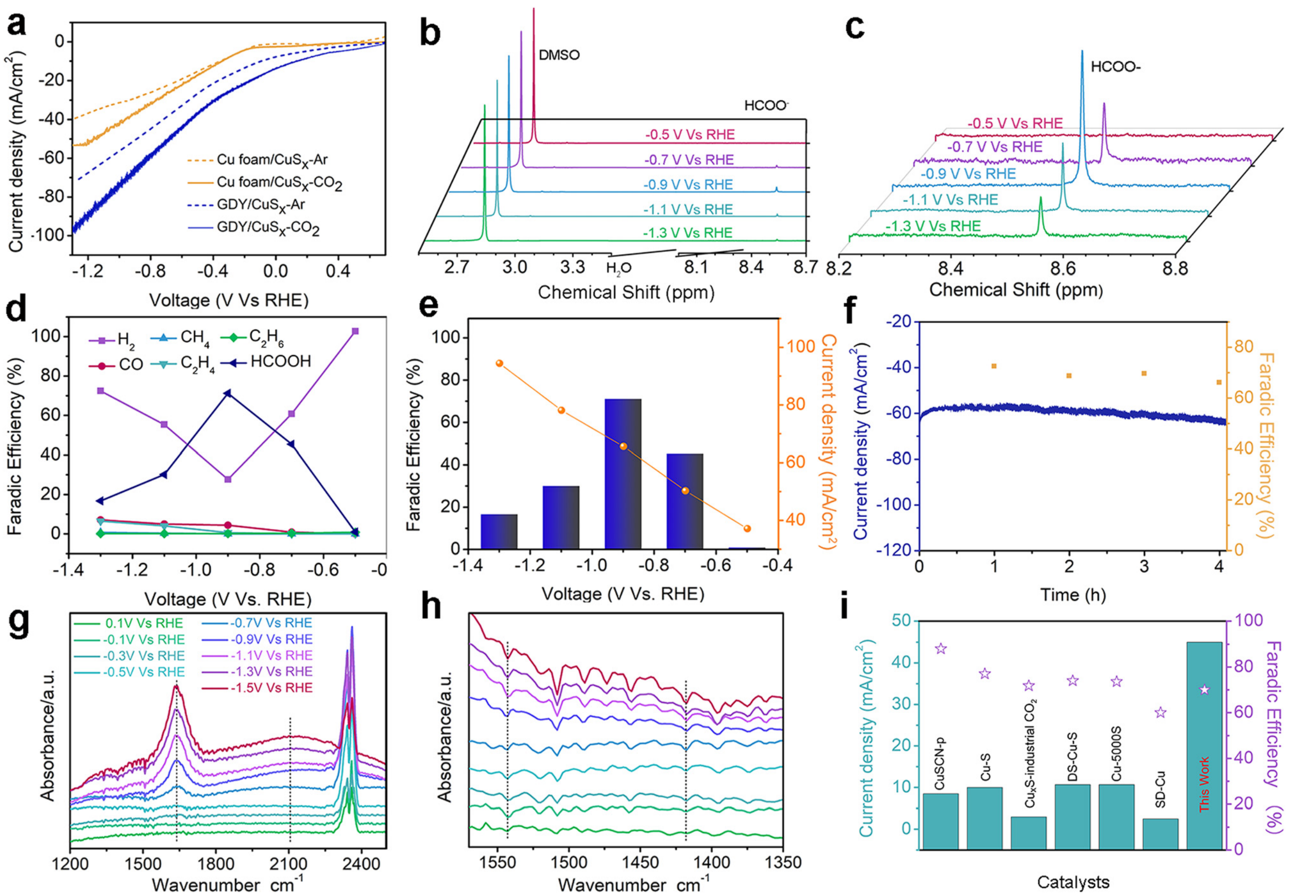

Fig. 4 (a) Linear sweep voltammetry of CuS_x and GDY/CuS_x recorded in CO_2- and Ar- saturated electrolytes. (b and c) ^{1}H NMR spectra of the electrolyte after the CO_2RR at the GDY/CuS_x electrode at different applied potentials. (d) Potential–faradaic efficiency (FE) curves for the products (HCOOH, H_2, CO, C_2H_4, and C_2H_6) produced during the CO_2RR on GDY/CuS_x. (e) Plot of FE and current density of GDY/CuS_x *vs.* the potential. (f) Stability and the corresponding faradaic efficiency for HCOOH produced with GDY/CuS_x at −0.9 V *vs.* RHE in CO_2-saturated 0.1 M $KHCO_3$. (g and h) Potential-dependent *in situ* ATR-FTIR spectra of the GDY/CuS_x electrode with CO_2 purging. (i) Comparison between GDY/CuS_x and reported Cu-based electrodes for the CO_2RR.

corresponds to the adsorbed CO (CO_{ads}) molecules and adsorbed carbonate on the electrode surface.[48–50] During the electrolysis process, the CO product ratio was low, which indicates that CO_{ads} was tightly bound to the surface with a low desorption rate. In Fig. 4h, the bands at 1544 and 1420 cm^{-1}, corresponding to the desorption of carbonate and the desorption of *COOH (carboxylate)/HCOO* (formate),[51] are absent. The absence of the HCOO* and CO_{ads} adsorption bands and the low selectivity for CO indicate that the main formation mechanism of formate is mainly through the reaction of physiosorbed CO_2 with H_{ads} ($CO_2 + H_{ads} + e^- \rightarrow HCOO^-$).[49,52] The Pourbaix diagram of the Cu–S system calculated by Liu *et al.*[53] indicated that S is unable to exist stably at the potential of formic acid production and will dissolve in the electrolyte.[49,53] Some monodisperse S will remain, and this residual S exists in substitutive form during the CO_2RR due to the sluggish reaction kinetics.[52,54,55] These residual S species were supposed to be effective on CO* adsorption, so that specific surface reaction sites are blocked, and a solution-phase CO_2 reduction pathway occurs for highly selective HCOOH production. The CO_2-to-HCOOH performance reported is better than most other Cu-based catalysts (Fig. 4i). The unique incomplete charge transfer between GDY and metal atoms, and the high CO_2 affinity of GDY, can effectively increase the number of active sites and regulate the adsorption/desorption capacity of key reaction intermediates, achieving an efficient and stable CO_2-to-HCOOH conversion (Fig. 5).

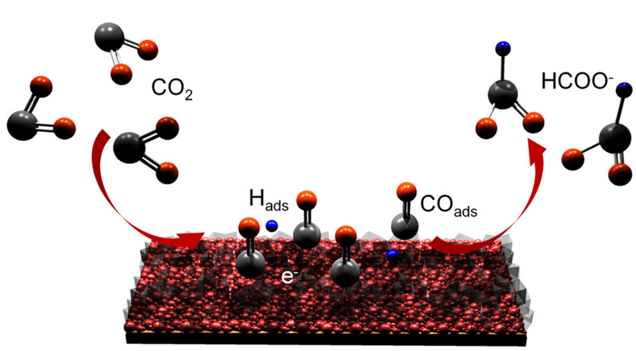

Fig. 5 Proposed reaction pathway of CO_2-to-HCOOH conversion.

Conclusions

In summary, we have developed an active CO_2-to-HCOOH heterostructured electrocatalyst of GDY/CuS_x *via* the *in situ* growth of GDY on the surface of CuS_x. The incomplete charge transfer between GDY and Cu atoms improved the catalyst conductivity, produced more active sites, and ultimately improved the catalytic performance. The faradaic efficiency of carbon dioxide reduction to formic acid reaches 70%, and a total current density of 65.6 mA cm^{-2} at −0.9 V *vs.* RHE is achieved. This work provides an effective strategy to enhance the selective catalysis of formate over low-cost Cu-based catalysts and expands the material options to produce this commercially valuable fuel and chemical.

Author contributions

Y. Li, Y. Xue, and S. Cao conceived the experiments. S. Cao performed the experiments. S. Cao and Y. Xue wrote the manuscript. Y. Li revised the manuscript. X. Chen, C. Zhang and Y. Gao helped with the electrochemical test and the *in situ* ATR-FTIR. All the authors discussed the results and commented on the manuscript.

Conflicts of interest

There are no conflicts to declare.

Acknowledgements

The authors acknowledge funding from the National Key Research and Development Project of China (2018YFA0703501), the National Natural Science Foundation of China (22021002), the Key Program of the Chinese Academy of Sciences (XDPB13), and the Beijing National Laboratory for Molecular Sciences (2020BMS20040).

References

1 T. J. Battin, S. Luyssaert, L. A. Kaplan, A. K. Aufdenkampe, A. Richter and L. J. Tranvik, The boundless carbon cycle, *Nat. Geosci.*, 2009, **2**, 598–600.
2 M. Reichstein, M. Bahn, P. Ciais, D. Frank, M. D. Mahecha, S. I. Seneviratne, J. Zscheischler, C. Beer, N. Buchmann, D. C. Frank, D. Papale, A. Rammig, P. Smith, K. Thonicke, M. van der Velde, S. Vicca, A. Walz and M. Wattenbach, Climate extremes and the carbon cycle, *Nature*, 2013, **500**, 287–295.
3 N. Mac Dowell, P. S. Fennell, N. Shah and G. C. Maitland, The role of CO_2 capture and utilization in mitigating climate change, *Nat. Clim. Change*, 2017, **7**, 243–249.
4 C. Liu, B. C. Colon, M. Ziesack, P. A. Silver and D. G. Nocera, Water splitting-biosynthetic system with CO_2 reduction efficiencies exceeding photosynthesis, *Science*, 2016, **352**, 1210–1213.
5 R. Sun, Y. Liao, S.-T. Bai, M. Zheng, C. Zhou, T. Zhang and B. F. Sels, Heterogeneous catalysts for CO_2 hydrogenation to formic acid/formate: from nanoscale to single atom, *Energy Environ. Sci.*, 2021, **14**, 1247–1285.
6 M. Grasemann and G. Laurenczy, Formic acid as a hydrogen source – recent developments and future trends, *Energy Environ. Sci.*, 2012, **5**, 8171–8181.
7 B. Loges, A. Boddien, H. Junge and M. Beller, Controlled generation of hydrogen from formic acid amine adducts at room temperature and application in H_2/O_2 fuel cells, *Angew. Chem., Int. Ed.*, 2008, **47**, 3962–3965.
8 P. Saha, S. Amanullah and A. Dey, Selectivity in electrochemical CO_2 reduction, *Acc. Chem. Res.*, 2022, **55**, 134–144.
9 S. Zhang, Q. Fan, R. Xia and T. J. Meyer, CO_2 reduction:from homogeneous to heterogeneous electrocatalysis, *Acc. Chem. Res.*, 2020, **53**, 255–264.
10 O. S. Bushuyev, P. De Luna, C. T. Dinh, L. Tao, G. Saur, J. van de Lagemaat, S. O. Kelley and E. H. Sargent, What should we make with CO_2 and how can we make it?, *Joule*, 2018, **2**, 825–832.
11 A. G. A. Mohamed, E. Zhou, Z. Zeng, J. Xie, D. Gao and Y. Wang, Asymmetric Oxo-bridged ZnPb bimetallic electrocatalysis boosting CO_2 -to-HCOOH reduction, *Adv. Sci.*, 2022, **9**, e2104138.
12 J. Wang, T. Xia, L. Wang, X. Zheng, Z. Qi, C. Gao, J. Zhu, Z. Li, H. Xu and Y. Xiong, Enabling visible-light-driven selective CO_2 reduction by doping quantum dots: trapping electrons and suppressing H_2 evolution, *Angew. Chem., Int. Ed.*, 2018, **57**, 16447–16451.
13 Z. Chen, K. Mou, X. Wang and L. Liu, Nitrogen-doped graphene quantum dots enhance the activity of Bi_2O_3 nanosheets for electrochemical reduction of CO_2 in a wide negative potential region, *Angew. Chem., Int. Ed.*, 2018, **57**, 12790–12794.
14 H. Luo, B. Li, J. G. Ma and P. Cheng, Surface modification of nano-Cu_2O for controlling CO_2 electrochemical reduction to ethylene and syngas, *Angew. Chem., Int. Ed.*, 2022, **61**, e202116736.
15 G. Li, Y. Li, H. Liu, Y. Guo, Y. Li and D. Zhu, Architecture of graphdiyne nanoscale films, *Chem. Commun.*, 2010, **46**, 3256–3258.
16 F. He and Y. Li, Advances on theory and experiments of the energy applications in graphdiyne, *CCS Chem.*, 2022, **0**, 1–23.
17 C. Huang, Y. Li, N. Wang, Y. Xue, Z. Zuo, H. Liu and Y. Li, Progress in research into 2D graphdiyne-based materials, *Chem. Rev.*, 2018, **118**, 7744–7803.
18 Y. Fang, Y. Liu, L. Qi, Y. Xue and Y. Li, 2D graphdiyne: an emerging carbon material, *Chem. Soc. Rev.*, 2022, **51**, 2681–2709.
19 X. Gao, H. Liu, D. Wang and J. Zhang, Graphdiyne: synthesis, properties, and applications, *Chem. Soc. Rev.*, 2019, **48**, 908–936.
20 R. Matsuoka, R. Sakamoto, K. Hoshiko, S. Sasaki, H. Masunaga, K. Nagashio and H. Nishihara, Crystalline graphdiyne nanosheets produced at a gas/liquid or liquid/liquid interface, *J. Am. Chem. Soc.*, 2017, **139**, 3145–3152.
21 Z. Zheng, Y. Xue and Y. Li, A new carbon allotrope: graphdiyne, *Trends Chem.*, 2022, **4**, 754–768.
22 Y. Liu, Y. Gao, F. He, Y. Xue and Y. Li, Controlled growth interface of charge transfer salts of nickel-7,7,8,8-

tetracyanoquinodimethane on surface of graphdiyne, *CCS Chem.*, 2022, **0**, 1–11.

23 Y. Gao, Y. Xue, L. Qi, C. Xing, X. Zheng, F. He and Y. Li, Rhodium nanocrystals on porous graphdiyne for electrocatalytic hydrogen evolution from saline water, *Nat. Commun.*, 2022, **13**, 5227.

24 Y. Gao, Y. Xue, F. He and Y. Li, Controlled growth of a high selectivity interface for seawater electrolysis, *Proc. Natl. Acad. Sci. U. S. A.*, 2022, **119**, e2206946119.

25 H. Yu, Y. Xue, L. Hui, C. Zhang, Y. Fang, Y. Liu, X. Chen, D. Zhang, B. Huang and Y. Li, Graphdiyne-based metal atomic catalysts for synthesizing ammonia, *Natl. Sci. Rev.*, 2021, **8**, nwaa213.

26 Y. Fang, Y. Xue, L. Hui, H. Yu and Y. Li, Graphdiyne@Janus magnetite for photocatalytic nitrogen fixation, *Angew. Chem., Int. Ed.*, 2021, **60**, 3170–3174.

27 H. Yu, Y. Xue, L. Hui, C. Zhang, Y. Li, Z. Zuo, Y. Zhao, Z. Li and Y. Li, Efficient hydrogen production on a 3D flexible heterojunction material, *Adv. Mater.*, 2018, **30**, e1707082.

28 L. Hui, Y. Xue, H. Yu, Y. Liu, Y. Fang, C. Xing, B. Huang and Y. Li, Highly efficient and selective generation of ammonia and hydrogen on a graphdiyne-based catalyst, *J. Am. Chem. Soc.*, 2019, **141**, 10677–10683.

29 Y. Xue, B. Huang, Y. Yi, Y. Guo, Z. Zuo, Y. Li, Z. Jia, H. Liu and Y. Li, Anchoring zero valence single atoms of nickel and iron on graphdiyne for hydrogen evolution, *Nat. Commun.*, 2018, **9**, 1460.

30 Y. Fang, Y. Xue, Y. Li, H. Yu, L. Hui, Y. Liu, C. Xing, C. Zhang, D. Zhang, Z. Wang, X. Chen, Y. Gao, B. Huang and Y. Li, Graphdiyne interface engineering: highly active and selective ammonia synthesis, *Angew. Chem., Int. Ed.*, 2020, **59**, 13021–13027.

31 Z. Wang, Z. Zheng, Y. Xue, F. He and Y. Li, Acidic water oxidation on quantum dots of IrO_x/graphdiyne, *Adv. Energy Mater.*, 2021, **11**, 2101138.

32 Y. Du, W. Zhou, J. Gao, X. Pan and Y. Li, Fundament and application of graphdiyne in electrochemical energy, *Acc. Chem. Res.*, 2020, **53**, 459–469.

33 Y. Xue, Y. Li, J. Zhang, Z. Liu and Y. Zhao, 2D graphdiyne materials: challenges and opportunities in energy field, *Sci. China: Chem.*, 2018, **61**, 765–786.

34 Z. Zuo, D. Wang, J. Zhang, F. Lu and Y. Li, Synthesis and applications of graphdiyne-based metal-free catalysts, *Adv. Mater.*, 2019, **31**, e1803762.

35 Y. Xue, L. Hui, H. Yu, Y. Liu, Y. Fang, B. Huang, Y. Zhao, Z. Li and Y. Li, Rationally engineered active sites for efficient and durable hydrogen generation, *Nat. Commun.*, 2019, **10**, 2281.

36 C. Xing, Y. Xue, B. Huang, H. Yu, L. Hui, Y. Fang, Y. Liu, Y. Zhao, Z. Li and Y. Li, Fluorographdiyne: A metal-free catalyst for applications in water reduction and oxidation, *Angew. Chem., Int. Ed.*, 2019, **58**, 13897–13903.

37 Z. Zheng, L. Qi, Y. Xue and Y. Li, Highly selective and durable of monodispersed metal atoms in ammonia production, *Nano Today*, 2022, **43**, 101431.

38 X. Zheng, Y. Xue, C. Zhang and Y. Li, Controlled growth of multidimensional interface for high-selectivity ammonia production, *CCS Chem.*, 2022, **0**, 1–10.

39 X. Luan, Z. Zheng, S. Zhao, Y. Xue and Y. Li, Controlled growth of the interface of $CdWO_x$/GDY for hydrogen energy conversion, *Adv. Funct. Mater.*, 2022, **32**, 2202843.

40 L. Qi, Z. Zheng, C. Xing, Z. Wang, X. Luan, Y. Xue, F. He and Y. Li, 1D nanowire heterojunction electrocatalysts of $MnCo_2O_4$/GDY for efficient overall water splitting, *Adv. Funct. Mater.*, 2021, **32**, 2107179.

41 Y. Zhao, J. Wan, H. Yao, L. Zhang, K. Lin, L. Wang, N. Yang, D. Liu, L. Song, J. Zhu, L. Gu, L. Liu, H. Zhao, Y. Li and D. Wang, Few-layer graphdiyne doped with sp-hybridized nitrogen atoms at acetylenic sites for oxygen reduction electrocatalysis, *Nat. Chem.*, 2018, **10**, 924–931.

42 K. Ma, J. Wu, X. Wang, Y. Sun, Z. Xiong, F. Dai, H. Bai, Y. Xie, Z. Kang and Y. Zhang, Periodically interrupting bonding behavior to reformat delocalized electronic states of graphdiyne for improved electrocatalytic hydrogen evolution, *Angew. Chem., Int. Ed.*, 2022, **61**, e202211094.

43 X. Gao, J. Zhou, R. Du, Z. Xie, S. Deng, R. Liu, Z. Liu and J. Zhang, Robust superhydrophobic foam: a graphdiyne-based hierarchical architecture for oil/water separation, *Adv. Mater.*, 2016, **28**, 168–173.

44 Y. Y. Han, X. L. Lu, S. F. Tang, X. P. Yin, Z. W. Wei and T. B. Lu, Metal-free 2D/2D heterojunction of graphitic carbon nitride/graphdiyne for improving the hole mobility of graphitic carbon nitride, *Adv. Energy Mater.*, 2018, **8**, 1702992.

45 J. Li, X. Gao, B. Liu, Q. Feng, X. B. Li, M. Y. Huang, Z. Liu, J. Zhang, C.-H. Tung and L.-Z. Wu, Graphdiyne: a metal-free material as hole transfer layer to fabricate quantum dot-sensitized photocathodes for hydrogen production, *J. Am. Chem. Soc.*, 2016, **138**, 3954–3957.

46 H. Zhong, M. Ghorbani-Asl, K. H. Ly, J. Zhang, J. Ge, M. Wang, Z. Liao, D. Makarov, E. Zschech, E. Brunner, I. M. Weidinger, J. Zhang, A. V. Krasheninnikov, S. Kaskel, R. Dong and X. Feng, Synergistic electroreduction of carbon dioxide to carbon monoxide on bimetallic layered conjugated metal-organic frameworks, *Nat. Commun.*, 2020, **11**, 1409.

47 E. R. Corson, R. Kas, R. Kostecki, J. J. Urban, W. A. Smith, B. D. McCloskey and R. Kortlever, In situ ATR–SEIRAS of carbon dioxide reduction at a plasmonic silver cathode, *J. Am. Chem. Soc.*, 2020, **142**, 11750–11762.

48 S. Zhu, T. Li, W.-B. Cai and M. Shao, CO_2 electrochemical reduction as probed through infrared spectroscopy, *ACS Energy Lett.*, 2019, **4**, 682–689.

49 K. R. Phillips, Y. Katayama, J. Hwang and Y. Shao-Horn, Sulfide-derived copper for electrochemical conversion of CO_2 to formic acid, *J. Phys. Chem. Lett.*, 2018, **9**, 4407–4412.

50 J. Heyes, M. Dunwell and B. Xu, CO_2 reduction on Cu at low overpotentials with surface-enhanced in situ spectroscopy, *J. Phys. Chem. C*, 2016, **120**, 17334–17341.

51 W. Deng, L. Zhang, L. Li, S. Chen, C. Hu, Z.-J. Zhao, T. Wang and J. Gong, Crucial role of surface hydroxyls on the activity and stability in electrochemical CO_2 reduction, *J. Am. Chem. Soc.*, 2019, **141**, 2911–2915.

52 T. Cheng, H. Xiao and W. A. Goddard, III, Reaction mechanisms for the electrochemical reduction of CO_2 to CO and formate on the Cu(100) surface at 298 K from quantum mechanics free energy calculations with explicit water, *J. Am. Chem. Soc.*, 2016, **138**, 13802–13805.
53 D. Liu, Y. Liu and M. Li, Understanding how atomic sulfur controls the selectivity of the electroreduction of CO_2 to formic acid on metallic Cu surfaces, *J. Phys. Chem. C*, 2020, **124**, 6145–6153.
54 Y. Deng, Y. Huang, D. Ren, A. D. Handoko, Z. W. Seh, P. Hirunsit and B. S. Yeo, On the role of sulfur for the selective electrochemical reduction of CO_2 to formate on CuS_x catalysts, *ACS Appl. Mater. Interfaces*, 2018, **10**, 28572–28581.
55 J. S. Yoo, R. Christensen, T. Vegge, J. K. Norskov and F. Studt, Theoretical insight into the trends that guide the electrochemical reduction of carbon dioxide to formic acid, *ChemSusChem*, 2016, **9**, 358–363.